Journal of Non-Crystalline Solids 481 (2018) 503–511

Contents lists available at ScienceDirect

Journal of Non-Crystalline Solids

journal homepage: www.elsevier.com/locate/jnoncrysol

Lateral deformation and defect resistance of compacted silica glass: Quantification of the scratching hardness of brittle glasses

Shigeki Sawamura[a,b], René Limbach[a], Harald Behrens[c], Lothar Wondraczek[a,*]

[a] Otto Schott Institute of Materials Research, Friedrich Schiller University Jena, Fraunhoferstrasse 6, D-07743 Jena, Germany
[b] Asahi Glass Co., Ltd., 1150 Hazawa-cho, Kanagawa-ku, Yokohama-shi, Kanagawa 221-8755, Japan
[c] Department of Mineralogy, Leibniz University of Hannover, Calinstrasse 3, D-30167 Hannover, Germany

ARTICLE INFO

Keywords:
Glass
Scratch resistance
Scratch hardness
Silica

ABSTRACT

Human interaction with multimedia devices occurs predominantly over inorganic glass surfaces. Scratch-induced damage is a primary limitation in the suitability of brittle glasses for this purpose. However, neither truly quantitative data nor a topo-chemical understanding of the underlying deformation process which would allow for the development of improved materials is presently available.

Here, we present lateral nano-indentation experiments for determining the work of deformation which is involved in the process of glass scratching. Using a series of hot-compressed vitreous silica with mild degrees of structural densification, we derive relations between quantitative scratch hardness and the underlying glass structure. We show that Young's modulus provides a clear rational for the observed variations in scratching hardness. In the specific case of silica, the energy needed to generate a certain scratch volume corresponds to roughly one tenth of Young's modulus. This relationship formally indicates that only about one tenth of the bonds which are involved in the deformation process are broken in its course. However, comparison with a more complex glass material with a certain fraction of two dimensional structural units and a strong ability for topological adaption to local stress clearly indicates a deviation from this behavior. This opens a pathway to topo-chemical engineering of scratch-resistant glasses.

1. Introduction

Despite the intriguing promise of extremely high intrinsic strength, glasses remain ultimately brittle and usually break in catastrophic ways, even when handled with care [1]. This apparent discrepancy has triggered major efforts in the field of glass chemistry, aiming at the conundrum of plastic deformation and local dissipation of mechanical energy in brittle materials. It is assumed that through tailoring of chemical composition and, thus, network topology of the solid glass (denoted topo-chemistry in the following), the formation and growth of defects which act as stress amplifiers [2] can be avoided on atomic level and, thus, stronger glasses can be derived [3]. Such a tailoring of chemical composition would be a major breakthrough of the field, both in terms of fundamental understanding and application, where glasses have always been enabling materials in societal progress. For example, human interaction with multimedia devices today occurs predominantly over inorganic glass surfaces. This holds for both haptic and visual contact, for example, on smartphones, tablet personal computers and other mobile or non-mobile electronic devices. In those, thin glass sheet is used as a protective cover, barrier and substrate material. Besides optical and chemical functions, it usually also determines the mechanical performance of the respective interactive display. Most critically, the glass component is to ensure high resistance to scratch damage which compromises optical appearance and, at the same time, presents the major source of strength-reducing surface flaws. Noteworthy, scratch damage may be induced at each stage of the lifecycle: besides actual use of the device, also during sheet production, packaging and transport, display manufacture or, e.g., component assembly. However, in contrast to the subject's fundamental importance, methods of physical quantification and the understanding of the topo-chemical basis of scratch-induced surface deformation are presently not well-developed, presenting a major obstacle in the exploration of glass surfaces with higher scratch resistance.

To date, scratch testing is conducted mostly in phenomenological ways [4–8]. These usually rely on applying a certain experimental protocol to produce a scratch, and examine the thus-created groove by visual inspection. In the archetype experiment a glass surface is scratched with a diamond stylus under monotonically increasing load. The fundamental regimes of plastic deformation, radial cracking, median or lateral cracking and chipping, and microabrasion are typically

* Corresponding author.
E-mail address: lothar.wondraczek@uni-jena.de (L. Wondraczek).

https://doi.org/10.1016/j.jnoncrysol.2017.11.035
Received 25 September 2017; Received in revised form 10 November 2017; Accepted 18 November 2017
Available online 30 November 2017

differentiated visually [4,9], and their onset is subsequently related to the normal load which was applied on the scratching device. More fundamental efforts to relate the defect resistance of glasses to their composition and structure, on the other hand, rely on normal indentation testing [3,10–12]. The hardness parameter which can be extracted from such experiments is strongly dependent on the experimental conditions. Its physical meaning and relation to material properties such as fracture toughness, brittleness or elasticity are therefore not readily visible. As an early consensus, it was derived that the indentation response of inorganic glasses results from the interplay of elastic deformation, structural compaction and shear [13–15]. Tailoring between these contributions has been assumed to enable the design of glasses with reduced brittleness and improved defect resistance [16]. More recently, however, it was noted that the structural reactions which underlie damage infliction are significantly more complex [17,18].

In terms of lateral deformation (which includes scratching, but also aspects of friction, wear and abrasion), some phenomenological understanding and correlation to chemical properties has been reached for reactive polishing or grinding processes with the goal to improve on the fabrication of optical-grade surfaces [17,19]. With some minor exceptions [9,20], systematic analysis of the scratching behavior itself remains largely limited to soda lime silicate glasses [6,20–24]. Rather than elucidating the chemical origin of deformation at the onset of scratching, however, these studies focused on the emergence of cracks, crack morphology and the underlying (transient) stress profiles [25]. A first notion of scratching hardness was derived by Yoshida et al. [26], using normal load and vertical contact area. Without entering into details, they suggested that the scratching hardness of glasses is related to the fracture mechanism, not the elastic behavior. Extending this view, fracture ultimately occurs at the limits of plastic deformation. Thus, the scratching hardness reflects the resistance of the considered material to plastic deformation during quasi-static lateral indentation. In the present report, we provide a chemical rational for this argument, determining initially the work of nanoscale lateral deformation across the plastic regime. Using the example of vitreous silica with different degrees of off-set compaction, we obtain a direct dependence of deformation work on Si−O bond density. This observation will enable the design of glassy materials with specific tribological properties using topo-chemical principles.

2. Materials and methods

For the present study, we selected silica as the archetype glass material with the highest degree of structural compressibility among all presently available oxide glasses. Its ability to compact originates from the large free volume and reflects in an exceptionally low Poisson ratio [27]. The structure of silica comprises tetrahedral units of $[SiO_4]^{4-}$ which are interconnected over all four edges to form a continuous network of ≡Si−O−Si≡ entities. The dominant super-structural units are six- to eight-fold rings of tetrahedra. Bonding is strongly covalent with the Si−O bond cleavage energy of 624 kJ/mol [28]. Fracture is usually assisted by adsorbed water [29], which reduces the energy of bond cleavage to 163 kJ/mol [28]. In order to test the structural dependence of lateral deformation, a set of samples is produced by compacting chemically equivalent glasses within the regime of congruent compression (< 1 GPa, see Fig. 1b) in which no changes occur in ion coordination or topology. This enables us to attribute variations in scratching hardness solely to variations in density.

2.1. Compression experiments

Compacted silica glass samples were prepared from commercially available Suprasil 2 fused silica (Heraeus Quarzglass GmbH & Co. KG) by isostatic compression in an internally heated gas pressure vessel, similar to the procedure described in Refs. [30–35], Fig. 1a. For this, individual bars of 5 × 5 × 25 mm^3 in size were directly loaded into the vessel and argon gas was employed as the compression medium. The glasses were heated at constant pressure up to a temperature of 1523 K, well above the glass transition temperature of T_g = 1393 K, and equilibrated for 12 min to allow for complete relaxation to the respective pressure. After equilibration above T_g, the glasses were cooled under pressure at a rate of 10 K/min down to room temperature. Using this method, silica glasses with frozen-in pressures of 100, 300 and 500 MPa were produced. For reference, also an uncompressed sample was made at 0.1 MPa, using the same time-temperature profile. Changes in the density ρ were evaluated using Archimedes' principle with dry ethanol as the immersion liquid. In order to minimize the influence of argon, which is expected to diffuse into the glass surface during the high-pressure treatments [32], the compacted glasses were subsequently grinded with silicon carbide paper and polished to optical finish using a water-based CeO suspension. The removed layer (~200 μm) was much thicker than the expected argon in-diffusion zone [36]. Following the approach of Davis et al. [37], infrared spectroscopic analysis revealed a total water content of around 490 ± 13 ppm in all glasses, independent of the applied compression conditions.

2.2. Nano-indentation under normal load

Indentation experiments were conducted through instrumented nano-indentation (G200, Agilent Inc.), using a Berkovich diamond tip (Synton-MDP Inc.) and operating in the continuous stiffness measurement (CSM) mode. The instrument's frame compliance and tip area function were calibrated prior to the experiments on a fused silica reference glass sample (Corning 7980, Corning Inc.) with known elastic properties (Young's modulus E = 72 GPa and Poisson ratio ν = 0.18), using the method proposed by Oliver and Pharr [38]. On each glass specimen, five indentations with a depth limit of 2 μm were created at a constant strain-rate of 0.05 s^{-1}. The hardness H, defined as the load divided by the projected contact area of the indenter tip F_N/A_c, as well as Young's modulus E were continuously recorded as a function of the indentation depth d by applying a weak oscillation to the indenter tip (Δd = 2 nm, f = 45 Hz) [12]. The value of E was deduced from the reduced elastic modulus E_r, according to Ref. [39]:

$$E = (1-\nu^2)\left[\frac{1}{E_r} - \frac{1-\nu_i^2}{E_i}\right]^{-1}, \quad (1)$$

with E_i = 1141 GPa and ν_i = 0.07 of the diamond tip, respectively. Poisson ratios of the compacted silica glasses were calculated from the longitudinal ν_L and transversal ν_T sound wave velocities, which were determined by means of an echometer 1077 (Karl Deutsch GmbH & Co. KG), equipped with 8–12 MHz piezoelectric transducers:

$$\nu = \frac{v_L^2 - 2v_T^2}{2(v_L^2 - v_T^2)} \quad (2)$$

All nanoindentation experiments were conducted in laboratory air at ambient temperature of around 298 ± 3 K.

2.3. Lateral nano-indentation and scratch testing

Lateral deformation and defect initiation were initially characterized in a ramp-load scratch test using the same nano-indentation set-up as described above. This test comprises an indenter tip moving across the glass surface under monotonically increasing load. Meanwhile, both the indentation depth and the lateral force F_L were continuously recorded [9]. On every glass specimen, 16 ramp-load scratch tests were conducted across a length of L_s = 600 μm at a scratch speed of 50 μm/s using a Berkovich diamond indenter tip in edge-forward orientation. The peak load at the end of the scratch was set to 300 mN, resulting in a constant loading rate of 25 mN/s. Prior to each test, the pristine glass surface was pre-scanned with the Berkovich tip under a load of 50 μN.

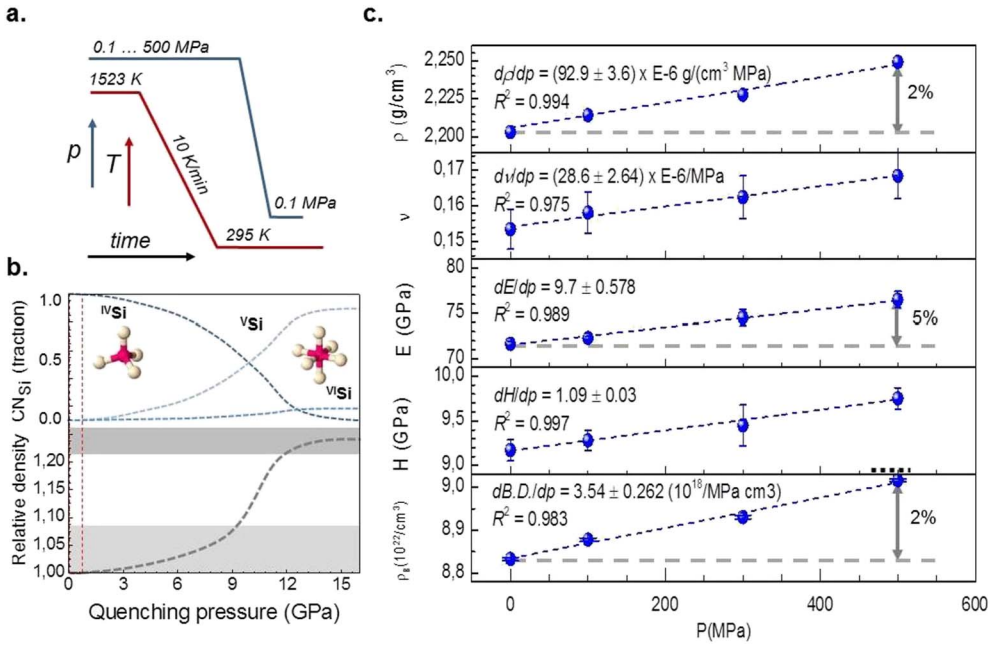

Fig. 1. (a) Experimental procedure of hot-compression of vitreous silica. (b) Schematic representation of the pressure-dependence of the Si speciation and density of vitreous silica: the present experiments were conducted in the highlighted low-pressure regime (red dashed line). (c) Physical and mechanical properties of silica glass as a function of the isostatic pressure p: density ρ, Poisson ratio ν, Young's modulus E, hardness H and network bond density ρ_B (see text for details). Error bars indicate standard deviations. The experimental errors for the density are smaller than the size of the symbols. Data shown in (b) were re-drawn from Ref. [61]. (For interpretation of the references to color in this figure legend, the reader is referred to the web version of this article.)

After scratching, a similar scan of the surface was conducted once again for evaluating of the size of the residual scratch groove.

In addition to the ramp-load tests, scratches with a total length of 200 µm were created under varying constant load with the objective to determine the work of deformation W_s required to scratch through a certain glass volume V_s. For this, the loads were adjusted to reach an anticipated indenter displacement (depth) into the surface layer of 500; 600 and 700 nm, respectively, using the data which were obtained from ramp-load scratch testing. Equivalent to the ramp-load scratch test, all constant-load scratching experiments were performed at a scratch speed of 50 µm/s using a Berkovich diamond indenter tip in edge-forward orientation. Three-dimensional data of scratch morphology were collected post mortem through wide-field confocal microscopy (Zeiss Smartproof 5, Zeiss). For judging the sensitivity of the evaluation procedure, an additional set of reference data was collected on a standard borosilicate glass (commercial Borofloat-33, Schott), denoted BS. The composition of this glass was $81SiO_2$-$13B_2O_3$-$2Al_2O_3$-$4Na_2O/K_2O$, with $\nu = 0.198 \pm 0.004$, $E = 61.1 \pm 0.2$ GPa and $H = 7.07 \pm 0.04$ GPa. Analyses were performed on the air-side of the pristine commercial glass. This particular reference was chosen because of the fundamentally different deformation behavior as compared to silica [12,15,40].

3. Results and discussion

3.1. Density and mechanical properties of compacted silica glass

Properties of the as-received compacted silica glasses are summarized in Table 1. Relationships between the isostatic pressure as employed during hot compression and the density as well as selected mechanical properties, including the Poisson ratio, Young's modulus and hardness are illustrated in Fig. 1c. Raising the pressure from 0.1 MPa (ambient) to 500 MPa increases the density almost linearly from 2.203 ± 0.001 g/cm^3 up to 2.249 ± 0.001 g/cm^3, i.e., a degree of compaction of up to roughly 2%. In comparison, the overall ability of permanent compaction of vitreous silica reaches as much as 21% under pressures in the 10 GPa range [27,41–43], eventually even higher when compaction is performed at elevated temperature [44]. The relatively low pressures applied in the present study limit the degree of densification $(\rho - \rho_0) / \rho_0$ (with the density at ambient pressure ρ_0, Table 1) to within the linear regime in which pressure-induced structural re-configuration is neglected (Fig. 1b). Nevertheless, some distinct variations in the mechanical performance are detected as a result of varying physical density. According to previous studies, the atomic packing density of glasses is directly related to the Poisson ratio, i.e., glasses with an open network structure typically exhibit lower values of ν than glasses more dense atomic packing [45,46]. Consequently, an increase of the Poisson ratio is expected as a result of compaction [47,48]. In the present case, a slight increase of the Poisson ratio from 0.153 ± 0.006 up to 0.168 ± 0.006 is seen for the silica glasses after the high-pressure treatment, confirming this expectation.

In addition to the Poisson ratio, also Young's modulus increases approximately linearly with increasing degree of compaction from 72.0 ± 0.3 GPa up to 75.9 ± 0.3 GPa. Likewise, the hardness increases from 9.17 ± 0.12 GPa up to 9.72 ± 0.07 GPa. Considering Young's modulus first, the observed tendency agrees very well with results from previous high-pressure studies not only on fused silica [44,47–49] but also on other glass families [49–52]. Hirao et al. [50] argued that the larger values of E noticed for $(50 - x)$MgO-xCaO-$50P_2O_5$ (x = 0; 25 and 50 mol%) glasses exposed to pressures of 6 GPa at elevated temperatures of $0.75T_g$ are attributed to the increased bond density in the permanently densified glasses. This conclusion was based on the early semi-empirical model of Makishima and Mackenzie [53], which considers the Young's modulus as a measure of the energy density stored inside the glass network. Following their concept, Young's

Table 1
Density ρ, densification $(\rho - \rho_0) / \rho_0$, atomic packing density C_g, Poisson ratio ν, Young's modulus E and hardness H of silica glass after hot compression at different isostatic pressures p.

p (MPa)	ρ (± 0.001 g/cm^3)	$(\rho - \rho_0) / \rho_0$ (%)	C_g	ν (± 0.006)	E (GPa)	H (GPa)
0.1	2.203	–	0.457	0.153	72.0 ± 0.3	9.17 ± 0.12
100	2.214	0.5	0.459	0.158	72.6 ± 0.5	9.28 ± 0.11
300	2.228	1.1	0.462	0.162	75.0 ± 0.5	9.54 ± 0.11
500	2.249	2.1	0.466	0.168	75.9 ± 0.3	9.72 ± 0.07

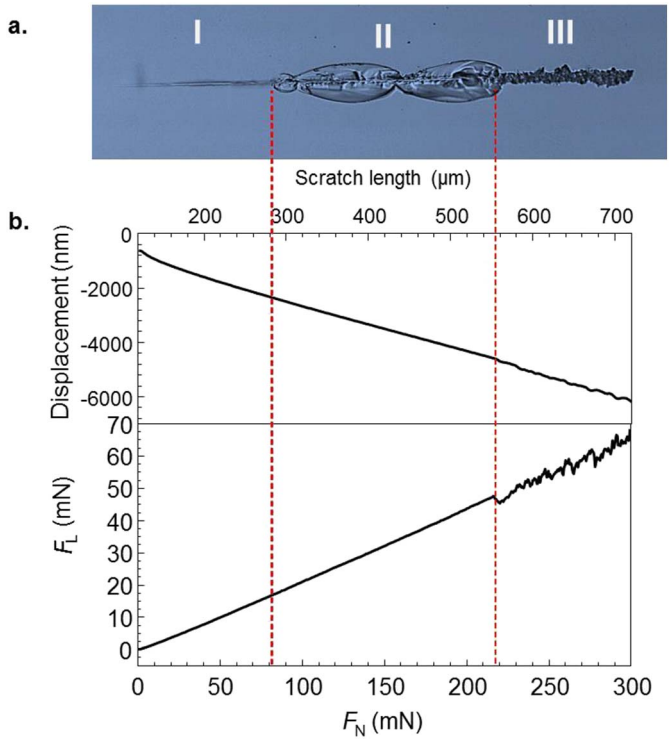

Fig. 2. Example of a ramp-load scratch test on uncompressed silica glass conducted with a Berkovich diamond tip in edge-forward orientation. (a) Optical micrograph of the resulting scratch pattern. (b) Indenter displacement h and lateral force F_L as a function of the applied load F_N, recorded by the nano-indenter. Dashed lines mark the onset of chipping (region II) and micro-abrasion (region III), as determined by optical inspection and derived from the first pop-in in the F_L curve, respectively.

modulus is determined from the atomic packing density C_g and the volume density of bonding, which is equal to the dissociation energy G_i of each single glass constituent, weighted by its molar fraction f_i,

$$E = 2C_g \sum f_i G_i \tag{3}$$

For a single-oxide glass such like fused silica, the atomic packing density $C_g = \rho V/M$ is estimated from the theoretical molar volume $V = 4/3\pi N(x{r_A}^3 + x{r_B}^3)$ occupied by the ions of the oxide A_xB_y, with the molar mass M, divided by the effective molar volume of the glass. The symbol N is the Avogadro number; r_A and r_B denote the radii of the involved cation (r_{Si} = 26 pm [28]) and oxygen anion (r_O = 135 pm [54]), respectively. The value of G_i for SiO_2 (68 kJ/cm^3) is tabulated in Ref. [55]. From Eq. (3) it is evident that an increase of the density in the absence of any compositional variations should lead to an equivalent increase of the atomic packing density (see Table 1) and by extension, Young's modulus of the glass. However, while the maximum densification of the silica glass compressed at p = 500 MPa is limited to about 2.1%, Young's modulus exceeds the value of the uncompressed glass specimen by about 5.4%. Such discrepancy has also been noticed, e.g., by Guerette et al. [44], though, its exact origin is not yet fully understood. We suppose that the difference between the pressure derivatives of ρ and E are related to higher sensitivity of the Young's modulus to structural modifications of the short- and medium-range order. The latter is usually not taken into account in the approach of Makishima and Mackenzie [45]. Therefore, large deviations between the predicted values of E and the experimental results may occur [56–60]. In principle, when silica glasses are subjected to sufficiently high pressure, a permanent densification of the glass network is achieved, on the one hand, through changes the bond angle distribution and, on the other hand, through variations in the ring statistics or silicon coordination number [34]. With respect to the low pressures applied in the current study, the latter effect may safely be excluded [61]. Instead, the congruent compaction of the glass network is more likely to involve a reduction of the Si—O—Si bond angles and the increase of smaller three- and four-membered silica rings at the expense of larger five- and six-membered silica rings [34]. The resulting strain also affects the effective energetics of the Si—O bond [28].

With these findings, not only the pressure-induced increase of the Young's modulus, but also the enhanced resistance against plastic deformation, as reflected by the hardness, can be explained. As already noted, it is widely assumed that the indentation deformation of glasses results from a competition between elastic deformation, densification and volume-conservative shear flow [62]. The relative contribution of the latter two processes varies strongly with the glass composition and is controlled by a complex interplay between the atomic packing density [14,63], network dimensionality [27] and the propensity for pressure-induced structural alterations at short- and medium-range order [18]. In silica glasses, densification is favored over shear-mediated plastic flow [64,65]. The underlying structural modifications which govern the densification of silica glasses during indentation are very probably equivalent to the mechanism responsible for the permanent compaction of the silicate network during isostatic compression [40,66]. With this in mind, the pre-densification of the silica glasses by hot compression is expected to diminish the ability to further densify during the subsequent indentation experiments by simply off-setting the degree of compaction. This results in an improved resistance against the penetration of sharp objects as mirrored by the observed hardness increase. This conclusion is well-supported by previous studies [67,68], where a considerably lower tendency towards densification was seen in glasses exposed to high pressures as compared to uncompressed references.

3.2. Ramp load scratch testing

As noted in the introduction, during a ramp-load scratch test on glass surfaces, the scratch morphology typically evolves from purely plastic deformation at low load (micro-ductile regime), to micro-cracking and chipping (micro-cracking regime) and, finally, abrasive wear (micro-abrasive regime) [4,9]. While only little systematic data is presently available, it seems that the loads required to activate each different regime depend to a large extent on the composition of the examined glass [5,26,69,70], but also on the scratching conditions, e.g., geometry and orientation of the indenter tip [71] or the scratching speed [9,24,71]. In the present case, ramp-load scratch tests with monotonically increasing loads from 50 μN up to 300 mN were performed. The resulting scratch pattern was initially evaluated by optical inspection. A typical such scratch pattern (created on the uncompressed reference glass) is presented in Fig. 2a. With progressively increasing load, a permanent scratch groove of increasing depth and width is created. In parallel, the lateral force needed to displace the scratching tip at constant speed also increases (Fig. 2b). At moderate load, frequent chipping occurs alongside the scratch, originating from the interaction between radial cracks and sub-surface lateral cracks reaching the glass surface [5]. Interestingly, this is hardly visible in the in situ recording of F_L, indicating that cracking occurs during unloading, i.e., when the tip has passed the respective zone of the scratch. At further increasing load, large amounts of debris mark the onset of the micro-abrasive regime. This, in turn, is readily visible in the F_L curve through the occurrence of sudden discontinuities and pop-ins [9]. The onset points of chipping and micro-abrasion are marked in Fig. 2.

When the normal load of scratching exceeds an onset value, the scratch pattern is determined by cracking reactions instead of plastic deformation. As cracking is largely affected by the presence of surface (and sub-surface) flaws and the resulting local amplification of acting stress, the onset values of chipping and micro-abrasion are distributed according to a certain probability function [5,9]. For the present case, this is shown in Fig. 3. The probability of defect formation increases with the applied load. A comparison among the silica glasses with

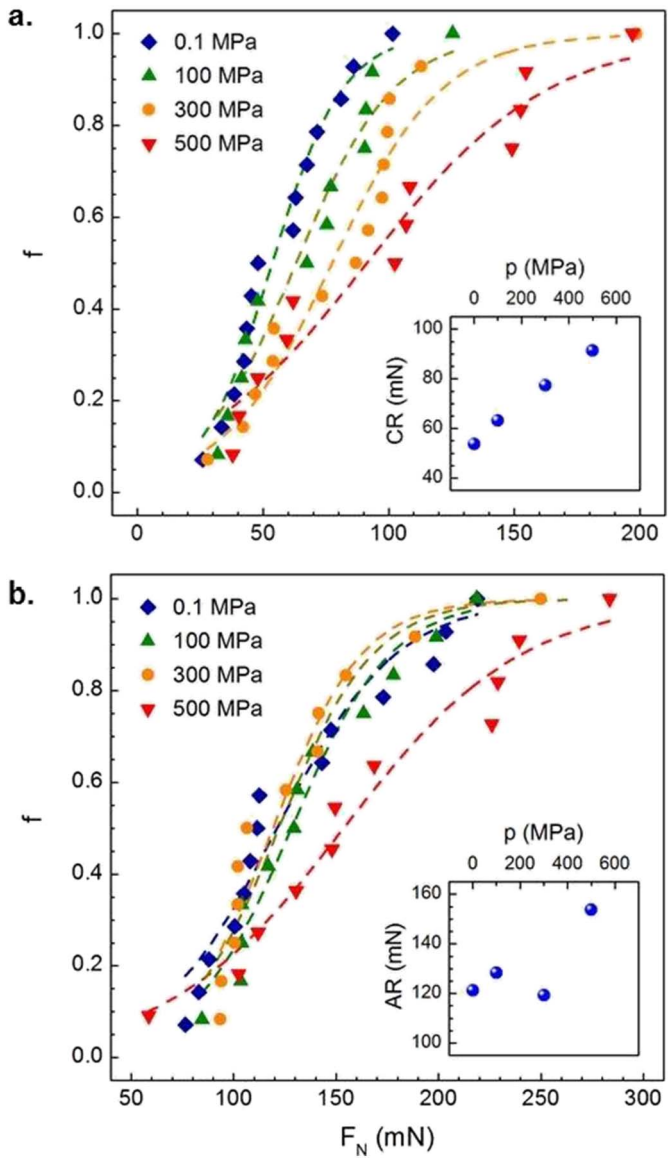

Fig. 3. Cumulative probability f of the load F_N at the onset of (a) chipping and (b) abrasion during ramp load scratch testing of silica glass as a function of the isostatic pressure p. Dashed lines are sigmoidal fits to the experimental results; the insets display the pressure-dependence of the chipping resistance CR and abrasion resistance AR, respectively, which are defined as the loads at a failure probability of 50%.

different grades of compaction reveals a gradual expansion of the cumulative distributions towards higher load. For example, chipping (Fig. 3a) starts at low loads of 26–102 mN in the uncompressed silica glass, whereas slightly higher loads of 38–197 mN are necessary to induce chipping in the sample compacted at p = 500 MPa. Likewise, the range of onset loads for the occurrence of micro-abrasion (Fig. 3b) increases from 77–219 mN (p = 0.1 MPa) to 86–263 mN (p = 500 MPa). This indicates a reduced susceptibility for both chipping and abrasive wear for the compacted samples. The trend among the individual datasets is very coherent in that an almost linear dependence is seen between the location of the 50th percentile for the normal load of chipping (CR) and micro-abrasion (AR), respectively, and the degree of compaction (insets of Fig. 3).

This result is obtained in analogy to the construct of indentation crack resistance as proposed by Kato et al. [72]. Fitting a sigmoidal function to the cumulative probability plot of the data, the load at which the failure probability reaches a value of 50% is approximated. Values of CR and AR are summarized in Table 2. The present results

Table 2
Chipping resistance CR, abrasion resistance AR, effective friction coefficient μ_{eff} and scratch hardness H_s of silica glass after hot compression under different isostatic pressures p.

p (MPa)	CR (mN)	AR (mN)	μ_{eff}	H_s (GPa)
0.1	54	121	0.209	6.71 ± 0.23
100	63	128	0.199	6.77 ± 0.18
300	77	119	0.196	6.97 ± 0.12
500	91	154	0.196	7.26 ± 0.17

suggest the creation of more defect resistant silica glasses as a result of compaction. This is a significant observation, as the reverse trend of a decreasing crack resistance has been noticed in previous studies involving normal indentation on isostatically compressed glasses [18,52,65,73–75]. This was rationalized through the reduced ability to further densify [15,16,72]. As a consequence, normal indentation cracking is initiated at lower load [67,68].

On first view, this apparent contradiction highlights the mechanistic difference between normal and lateral indentation testing. In particular, it clearly shows that conclusions on surface defect resistance from normal indentation testing are overly simplistic as they do not necessarily reflect the actual damage mechanism. According to earlier observations of Le Houérou et al. [5] derived from ramp-load scratch tests on a number of soda-lime silicate glasses of varying chemical composition, the probability of chipping is related to the atomic packing density of glasses. Apart from that, it was tentatively argued that the amount of non-bridging oxygen species in the respective glass type affects the type of fracture or slipping reaction in the vicinity of the scratching stylus. Also, a more open structure is usually more prone to water attack, which is a key parameter in the initiation of surface cracks [76]. As for the present case, we are considering a fully-polymerized network of silica tetrahedra in which the density is varied without varying the degree of polymerization. The observed decrease in the cumulative probability of chipping (or abrasive cracking) with increasing degree of compaction partially confirms Le Houérou's observations [5]. Similar but less pronounced observations as with chipping are also made on the occurrence of microabrasion.

Further insight is obtained from closer inspection of the data shown in Fig. 3. The actual difference between all curves lies in the steepness of the underlying probability function, not in the occasional onset values of cracking at low load. This means that the observed difference among the different samples (which is only on the high-load side) is very likely caused by a decrease in the likelihood for the scratching tip to intersect or initiate a crack-inducing flaw. Such a probability decrease can be a direct result of the hardness variation which is induced by compaction: compacted glasses exhibit higher hardness, thus, higher resistance against penetration of the employed Berkovich tip (Fig. 1c). For clarity, load-displacement curves are provided in Fig. 4a. The volume and surface area which are then probed by the indenter result directly from the geometry of the Berkovich tip. In the scratching experiment, the resulting scratch groove is wider (and deeper) at lower hardness. For example, the probed surface area (groove width) is about 5% smaller and the probability of finding a crack-inducing flaw decreases in the samples which were compacted at p = 500 MPa (Fig. 4b).

In consequence, when the lateral force rather than the normal load is considered in the analysis the above trend for AR disappears, Fig. 5a. For CR (Fig. 5b) which occurs at lower load, the trend of increasing resistance to lateral fracture with increasing degree of compaction remains present, although somewhat less pronounced.

Due to the strong dependence on experimental conditions and the presence of surface flaws, material insights from fracture experiments are strongly limited. The primary focus of the present report is therefore on the crack-free regime of scratching. As shown in Fig. 6, the present ramp-load tests exhibit a micro-ductile regime within the loading range of up to ~50 mN in which no cracking is observed and the relation

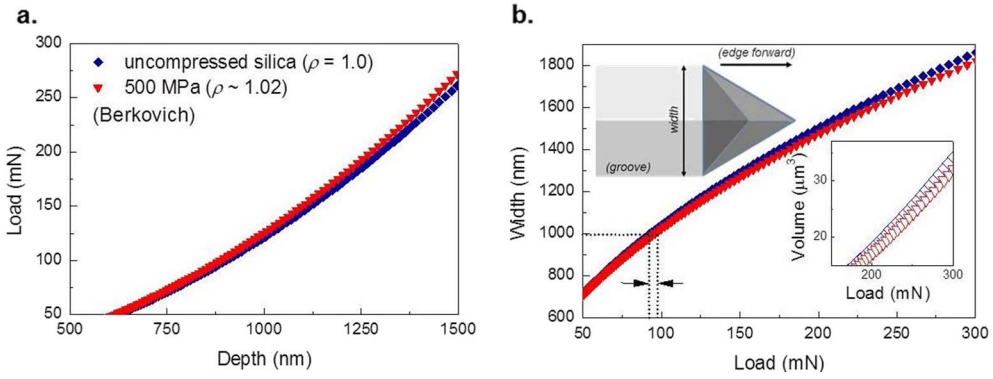

Fig. 4. (a) Indentation load-displacement curves for uncompressed silica and a glass hot-compressed at an isostatic pressure of p = 500 MPa. (b) Resulting width of the scratch groove during ramp-load scratch testing with a Berkovich diamond tip in edge-forward direction. The inset of (b) depicts the variation in indentation volume. For clarity, the difference in required load to generate a groove-width of 1000 nm is marked.

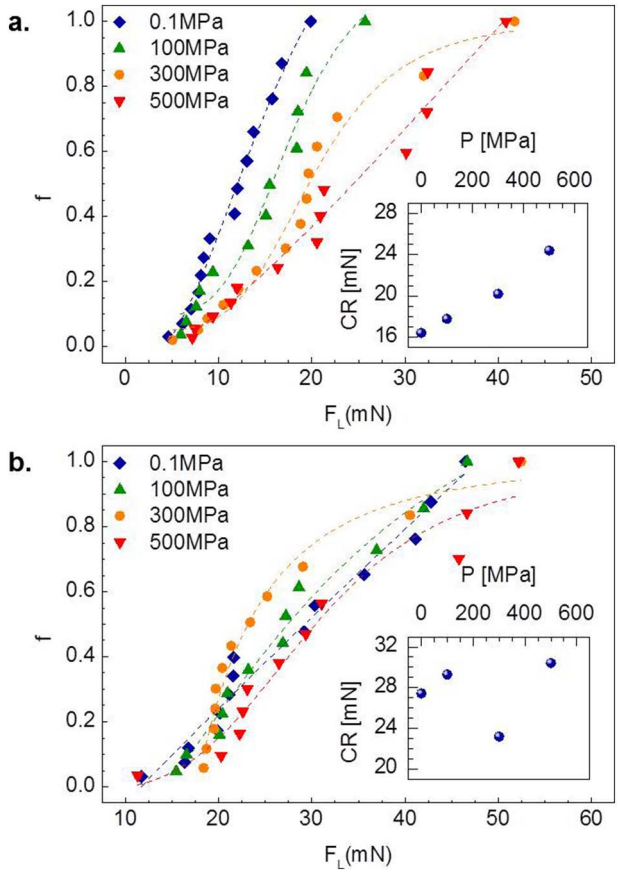

Fig. 5. Cumulative probability f of the lateral load F_L at the onset of (a) chipping and (b) abrasion during ramp load scratch testing of silica glass as a function of the isostatic pressure p. Dashed lines are sigmoidal fits to the experimental results and the insets display the pressure-dependence of the chipping CR and abrasion resistance AR, respectively, which are defined as the loads at a failure probability of 50%.

between lateral force and normal load is approximately linear. Increasing degree of structural compaction reduces the slope of the F_L-F_N curve and, hence, the effective friction coefficient $\mu_{eff} = F_L/F_N$ (inset of Fig. 6). According to Fig. 2, the scratch groove of this experiment is a result of elastic-plastic deformation. Thus, other than assumed in Coulomb's law, both adhesive and plowing forces contribute to the value of μ_{eff}. At present, we refrain from the effort of analytical separation of the two contributions due to the complex indenter geometry employed in the present study.

3.3. Constant load scratch testing

Following ramp-load testing, constant-load scratch tests were

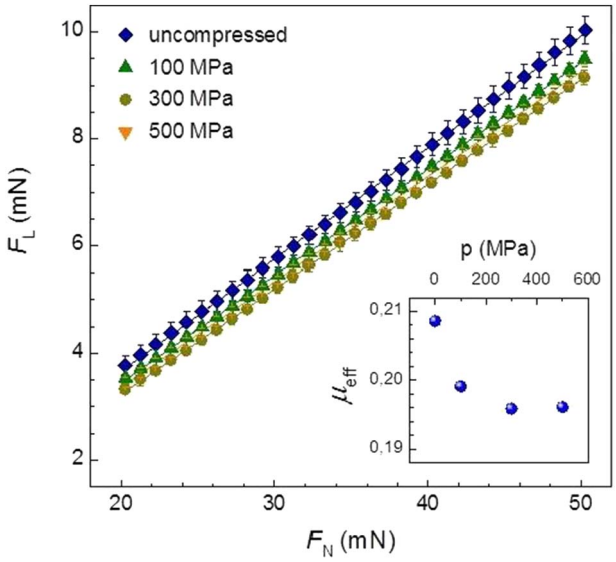

Fig. 6. Relationship between lateral force F_L and load F_N during ramp load scratch testing of silica glass as a function of the isostatic pressure p. The inset displays the pressure-dependence of the effective friction coefficient μ_{eff}, derived from the slope of linear regression of F_L over F_N.

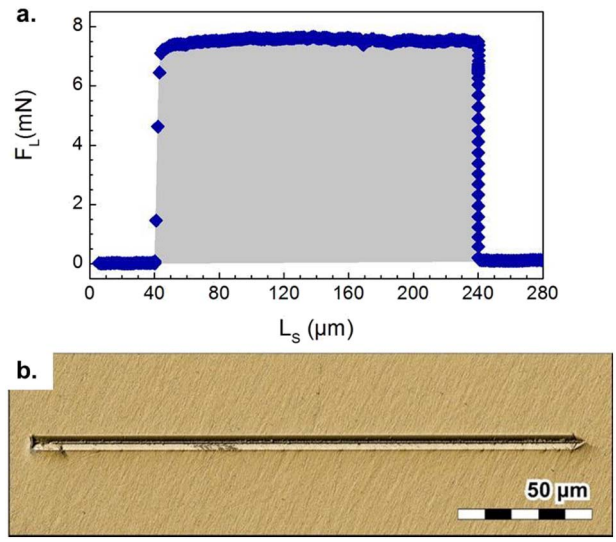

Fig. 7. Constant load (F_N = 45 mN) scratch test on uncompressed silica glass conducted with a Berkovich diamond tip in edge-forward orientation, showing (a) the lateral force F_L as recorded by the nano-indenter during displacement over a scratch length of L_s = 200 μm and (b) a confocal micrograph of the resulting scratch groove. The gray area corresponds to the work of deformation.

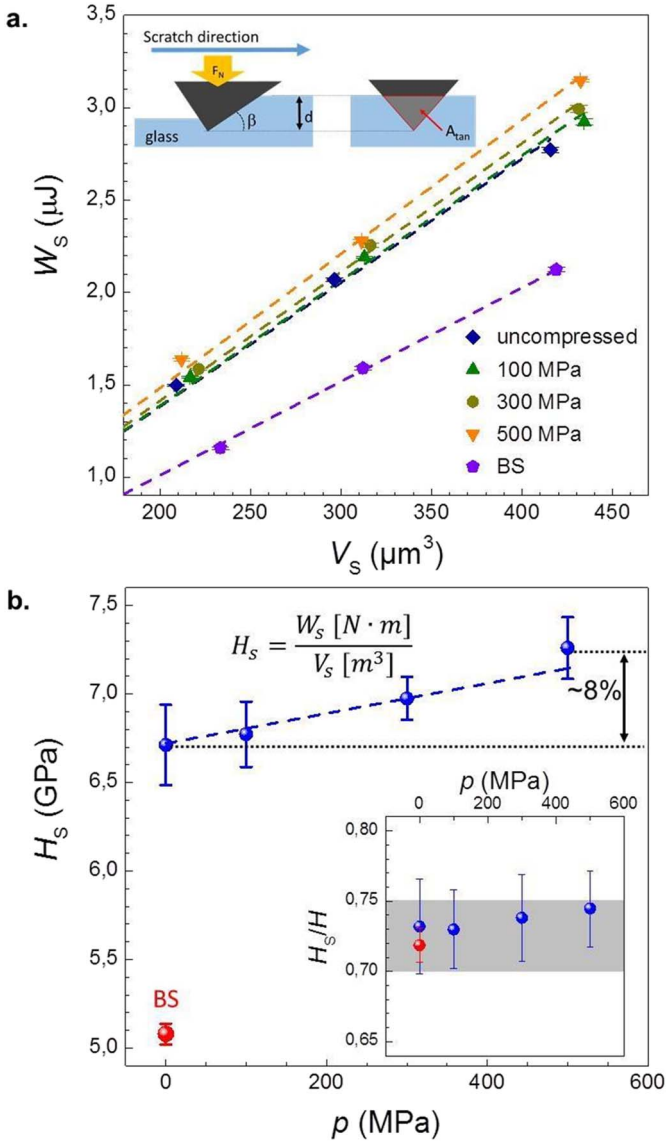

Fig. 8. (a) Relationship between the work of deformation W_s and the scratch volume V_s of silica glass as a function of the isostatic pressure p. The inset of (a) depicts the experimental set-up from which the value of V_s was derived (see text for details). (b) Pressure-dependence of the scratch hardness H_s, which was derived from the slope of linear regression of W_s over V_s. The inset displays the scratch hardness over the hardness H_s/H as a function of p. For comparison, the experimental data for a commercially available Borofloat 33 glass specimen, referred to as BS, was added.

performed within the region of elastic-plastic deformation. An example is provided in Fig. 7, using a load of 45 mN on uncompressed silica. The loading curve is given in Fig. 7a in terms of lateral force and displacement. Fig. 5b is a confocal micrograph of the corresponding scratch groove.

The effective work of deformation W_s is derived from the integral of $F_L dL$ across the length of the scratch L_s, $W_s = \int F_L dL_S$ (Fig. 8a). A first question is how sensitive this parameter is to even slight differences in glass structure. Due to the contribution of plowing friction, clearly, W_s strongly depends on the depth of the scratch groove and, thus, hardness of the material (see Fig. 4). We therefore determined the deformed volume V_s as the volume of the scratch groove during scratching (neglecting the occurrence of pile-up) and referenced W_s to V_s, $H_s = W_s / V_s$,

$$V_s = \int A_{tan} dl = \int \frac{\sqrt{3}\, d^2}{2 \tan \beta} dl \tag{4}$$

with the Berkovich edge-forward contact angle $\beta = 12.95°$ and the indentation depth d. Noteworthy, through this way of in situ evaluation, we integrate over both plastic and elastic contributions to deformation.

The value of H_s reflects the work required to deform a certain volume of material through scratching. As shown in Fig. 8a, within the examined range of normal load, there is a linear correlation between W_s and V_s and, thus, H_s is a constant parameter for each sample. In the following, H_s is denoted scratching hardness, corresponding to the similar use of this term by Yoshida et al. [14]. We find a clear, approximately linear dependence of H_s on the isostatic pressure employed during hot-compression (Fig. 8b), resulting in a relative increase of H_s by about 8% for the silica glass with the highest degree of compaction of about 2%. This compares to a normal hardness increase by about 6% under the same conditions. The relation between H_s and the regular (normal indentation) hardness H is shown in the inset of Fig. 8b. The absolute value of H_s/H clearly depends on experimental conditions and is, therefore, not discussed further at this stage. However, some significant conclusions can be drawn from the present observations: for one, there is no strong trend in the value of H_s/H as a function of silica density, within the range of observation. The slight increase of H_s/H which is seen with increasing isostatic pressure lies fully within the experimental accuracy. As a consequence, the scratching hardness H_s can be estimated directly from the normal hardness H. This observation, on the other hand, confirms our expectations that the present extent of compaction does not cause any major structural re-configuration besides congruent densification. Therefore, we do not expect variations in the principle mechanism of deformation which would facilitate (or prevent) lateral indentation over normal indentation.

For the second observation, we consider a typical borosilicate glass, referred to as BS. For comparison, data are included in Fig. 8. Here, a very clear difference is seen in W_s, in its volume dependence H_s and in the ratio of H_s/H. Most obviously, this shows that W_s is strongly sensitive to chemical composition, reflecting its applicability for discriminating the mechanical response of different glasses. Additionally, it suggests that H_s/H is composition-dependent, even though it appeared constant for the series of compacted silica glasses. This further signifies the complex relationship between scratch hardness and normal hardness. That is, structural parameters which are usually hidden within the notion of interacting contributions of compaction and shear have a different impact on normal and lateral indentation. For example, also in brittle glasses, lateral deformation is certainly affected by adhesive forces and stick-slip reactions which do not contribute to normal indentation. The present finding indicates that the dependence of these latter effects on molecular structure (as determined by chemical composition or thermo-mechanical history) is significant even within the narrow class of silicate glasses.

In Fig. 9, the value of H_s is related to the network bond density ρ_B. For the BS reference glass, the value of ρ_B is taken from the sum of the densities of Si—O, Al—O and ^{IV}B-O, assuming that only these bonds contribute to the formation of a three-dimensional glass network. This application has been chosen to obtain a qualitative view at the relation between the number of bonds which are involved in the scratching process and the observed scratching energy. BS is included in this analysis as a point of reference, for the moment ignoring the variation in bond strength as compared to the silica variants. As shown in Fig. 1c, in compacted silica glasses, the variation in network bond density is a direct result of network densification: there are no changes in network topology. Thus, with increasing degree of compaction, a linearly increasing number of bonds is involved in the deformation process. Consequently, also the scratch energy increases linearly. When comparing to the bulk energy, however, there is a difference of about one order of magnitude between both values for the compacted silica glasses as well as the BS reference glass. This result formally indicates that in ten involved bonds only one is broken during the process of deformation. Together with the previous observations, this particular finding gives rise to the conclusion that as a rough initial guide, the scratching hardness is about one tenth of Young's modulus for the

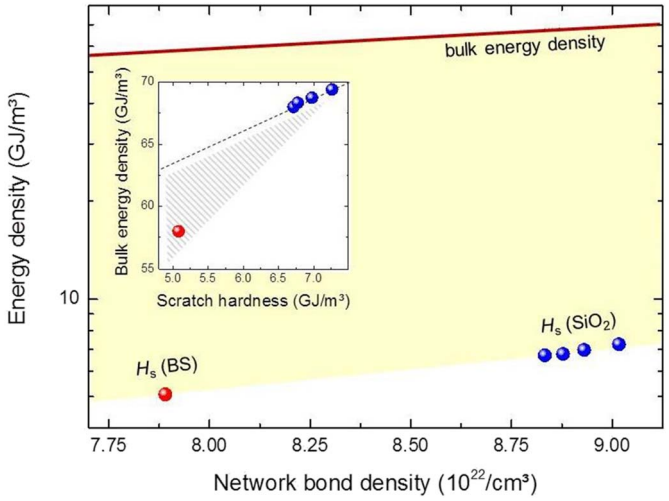

Fig. 9. Scratching hardness H_s as a function of network bond density ρ_B. As a guide for the eye, the bulk energy density is also shown. The inset displays the correlation between bulk energy and scratch hardness. The dashed line is a guide for the eye, indicating a linear dependence among the compacted silica glasses.

observed cases of compacted silica glass and the BS reference glass. In detail, however, the relation between H_s and E is clearly more complex (see inset of Fig. 9). This is certainly related to the increasing structural complexity of borosilicates and other glasses, which enable more complex topological reactions in answer to local mechanical load, opening a pathway to topo-chemical engineering of scratch-resistant glasses.

4. Conclusions

We used lateral nano-indentation for evaluating the fracture onset and the work of deformation which is involved in the process of glass scratching. For this, we employed lateral force analysis and path integration during ramp-load tests and constant-load tests on a series of hot-compressed vitreous silica glasses. The glasses exhibited mild degrees of structural densification, for which we derived relations between quantitative scratch hardness and the underlying glass structure. The density of network-forming bonds was identified as the primary factor in the resistance to lateral deformation. We show that Young's modulus provides a clear rational for the observed variations in scratching hardness. As a rule of thumb, the scratching energy density is roughly one tenth of Young's modulus. This formally indicates that only about one tenth of the bonds which are involved in the deformation process are broken in its course. However, comparing this observation to a more complex glass material with a certain fraction of two dimensional structural units and a strong ability for topological adaption to local stress clearly indicates a deviation from this behavior. This opens a pathway to topo-chemical engineering of scratch-resistant glasses.

Acknowledgements

This project has received funding from the European Research Council (ERC) under the European Union's Horizon 2020 research and innovation program (ERC grant UTOPES, grant agreement no. 681652).

References

[1] A. Kelly, Strong Solids, 2nd ed., Clarendon Pr, Oxford, 1973.
[2] A.A. Griffith, The phenomena of rupture and flow in solids, Philos. Trans. R. Soc. A Math. Phys. Eng. Sci. 221 (1921) 163–198.
[3] L. Wondraczek, J.C. Mauro, J. Eckert, U. Kühn, J. Horbach, J. Deubener, T. Rouxel, Towards ultrastrong glasses, Adv. Mater. 23 (2011) 4578–4586.
[4] V. Le Houérou, J.C. Sangleboeuf, T. Rouxel, Scratchability of soda-lime silica (SLS) glasses: dynamic fracture analysis, Key Eng. Mater. 290 (2005) 31–38.
[5] V. Le Houérou, J.C. Sangleboeuf, S. Dériano, T. Rouxel, G. Duisit, Surface damage of soda–lime–silica glasses: indentation scratch behavior, J. Non-Cryst. Solids 316 (2003) 54–63.
[6] P. Bandyopadhyay, A. Dey, S. Roy, N. Dey, A. Mukhopadhyay, Nanomechanical properties inside the scratch grooves of soda–lime–silica glass, Appl. Phys. A Mater. Sci. Process. 107 (2012) 943–948.
[7] J. Schneider, S. Schula, W.P. Weinhold, Characterisation of the scratch resistance of annealed and tempered architectural glass, Thin Solid Films 520 (2012) 4190–4198.
[8] K.H. Nielsen, S. Karlsson, R. Limbach, L. Wondraczek, Quantitative image analysis for evaluating the abrasion resistance of nanoporous silica films on glass, Sci. Rep. 5 (2015) 17708.
[9] E. Moayedi, L. Wondraczek, Quantitative analysis of scratch-induced microabrasion on silica glass, J. Non-Cryst. Solids 470 (2017) 138–144.
[10] M.M. Smedskjaer, J.C. Mauro, Y. Yue, Prediction of glass hardness using temperature-dependent constraint theory, Phys. Rev. Lett. 105 (2010) 115503.
[11] Morten M. Smedskjaer, Christian Hermansen, Randall E. Youngman, Topological engineering of glasses using temperature-dependent constraints, MRS Bull. 42 (2017) 29–33.
[12] R. Limbach, B.P. Rodrigues, L. Wondraczek, Strain-rate sensitivity of glasses, J. Non-Cryst. Solids 404 (2014) 124–134.
[13] M. Yamane, J.D. Mackenzie, Vicker's hardness of glass, J. Non-Cryst. Solids 15 (1974) 153–164.
[14] S. Yoshida, J.C. Sanglebœuf, T. Rouxel, Quantitative evaluation of indentation-induced densification in glass, J. Mater. Res. 20 (2005) 3404–3412.
[15] R. Limbach, A. Winterstein-Beckmann, J. Dellith, D. Möncke, L. Wondraczek, Plasticity, crack initiation and defect resistance in alkali-borosilicate glasses: from normal to anomalous behavior, J. Non-Cryst. Solids 417 (2015) 15–27.
[16] J. Sehgal, S. Ito, Brittleness of glass, J. Non-Cryst. Solids 253 (1999) 126–132.
[17] H.N. Li, T.B. Yu, L.D. Zhu, W.S. Wang, Evaluation of grinding-induced subsurface damage in optical glass BK7, J. Mater. Process. Technol. 229 (2016) 785–794.
[18] Kacper Januchta, Randall E. Youngman, Ashutosh Goel, Mathieu Bauchy, Stephan L. Logunov, Sylwester J. Rzoska, Michal Bockowski, Lars R. Jensen, Morten M. Smedskjaer, Discovery of ultra-crack-resistant oxide glasses with adaptive networks, Chem. Mater. 29 (2017) 5865–5876.
[19] M. Emberger, J. Koller, M. Laimer, M. Hell, K. Oender, A. Trost, M. Maass, W. Witte, H. Hintner, A.M. Lechner, Experimental investigation on grinding characteristics of optical glass BK7; with special emphasis on the effects of machining parameters, Int. J. Adv. Manuf. Technol. 82 (2011) 1405–1419.
[20] P. Bandyopadhyay, A.K. Mukhopadhyay, Role of shear stress in scratch deformation of soda-lime-silica glass, J. Non-Cryst. Solids 362 (2013) 101–113.
[21] P. Bandyopadhyay, A. Dey, S. Roy, A.K. Mukhopadhyay, Effect of load in scratch experiments on soda lime silica glass, J. Non-Cryst. Solids 358 (2012) 1091–1103.
[22] P. Bandyopadhyay, A. Dey, A. Mandal, N. Dey, S. Roy, A. Mukhopadhyay, Effect of scratching speed on deformation of soda–lime–silica glass, Appl. Phys. A Mater. Sci. Process. 107 (2012) 685–690.
[23] P. Bandyopadhyay, A. Dey, A.K. Mandal, N. Dey, A.K. Mukhopadhyay, New observations on scratch deformations of soda lime silica glass, J. Non-Cryst. Solids 358 (2012) 1897.
[24] P. Bandyopadhyay, A. Dey, A.K. Mukhopadhyay, Novel combined scratch and nanoindentation experiments on soda-lime-silica glass, Int. J. Appl. Glas. Sci. 3 (2012) 163–179.
[25] W. Wang, P. Yao, J. Wang, C. Huang, T. Kuriyagawa, H. Zhu, B. Zou, H. Liu, Elastic stress field model and micro-crack evolution for isotropic brittle materials during single grit scratching, Ceram. Int. 43 (2017) 10726–10736.
[26] S. Yoshida, H. Tanaka, T. Hayashi, J. Matsuoka, N. Soga, Scratch resistance of sodium borosilicate glass, J. Ceram. Soc. Jpn. 109 (2001) 511–515.
[27] T. Rouxel, H. Ji, T. Hammouda, A. Moréac, Poisson's ratio and the densification of glass under high pressure, Phys. Rev. Lett. 100 (2008) 225501.
[28] C. Hühn, A. Erlebach, D. Mey, L. Wondraczek, M. Sierka, Ab initio energetics of Si−O bond cleavage, J. Comput. Chem. (2017) 2349–2353.
[29] L. Wondraczek, A. Dittmar, C. Oelgardt, F. Célarié, M. Ciccotti, C. Marlière, Real-time observation of a non-equilibrium liquid condensate confined at tensile crack tips in oxide glasses, J. Am. Ceram. Soc. 89 (2006) 746–749.
[30] Y. Yue, L. Wondraczek, H. Behrens, J. Deubener, Glass transition in an isostatically compressed calcium metaphosphate glass, J. Chem. Phys. 126 (2007) 144902.
[31] L. Wondraczek, S. Sen, H. Behrens, R.E. Youngman, Structure-energy map of alkali borosilicate glasses: effects of pressure and temperature, Phys. Rev. B 76 (2007) 014202.
[32] L. Wondraczek, H. Behrens, Molar volume, excess enthalpy, and Prigogine-Defay ratio of some silicate glasses with different (P,T) histories, J. Chem. Phys. 127 (2007) 154503.
[33] S. Reibstein, L. Wondraczek, D. de Ligny, S. Krolikowski, S. Sirotkin, J.P. Simon, V. Martinez, B. Champagnon, Structural heterogeneity and pressure-relaxation in compressed borosilicate glasses by in situ small angle X-ray scattering, J. Chem. Phys. 134 (2011) 204502.
[34] S. Kapoor, L. Wondraczek, M.M. Smedskjaer, Pressure-induced densification of oxide glasses at the glass transition, Front Mater. 4 (2017) 1–20.
[35] L. Wondraczek, H. Behrens, Y. Yue, J. Deubener, G.W. Scherer, Relaxation and glass transition in an isostatically compressed diopside glass, J. Am. Ceram. Soc. 90 (2007) 1556–1561.
[36] H. Behrens, Ar, CO_2 and H_2O diffusion in silica glasses at 2 kbar pressure, Chem. Geol. 272 (2010) 40–48.
[37] K.M. Davis, A. Agarwal, M. Tomozawa, K. Hirao, Quantitative infrared spectroscopic measurement of hydroxyl concentrations in silica glass, J. Non-Cryst. Solids

203 (1996) 27–36.
[38] W.C. Oliver, G.M. Pharr, An improved technique for determining hardness and elastic modulus using load and displacement sensing indentation experiments, J. Mater. Res. 7 (1992) 1564–1583.
[39] K.L. Johnson, Contact Mechanics, Cambridge Univ. Press, Cambridge [u.a.], 2004 (transferred to digital print).
[40] A. Winterstein-Beckmann, D. Möncke, D. Palles, E.I. Kamitsos, L. Wondraczek, Raman spectroscopic study of structural changes induced by micro-indentation in low alkali borosilicate glasses, J. Non-Cryst. Solids 401 (2014) 110–114.
[41] M. Grimsditch, Polymorphism in amorphous SiO_2, Phys. Rev. Lett. 52 (1984) 2379–2381.
[42] S. Susman, K.J. Volin, D.L. Price, M. Grimsditch, J.P. Rino, R.K. Kalia, P. Vashishta, G. Gwanmesia, Y. Wang, R.C. Liebermann, Intermediate-range order in permanently densified vitreous ${\mathrm{SiO}}_{2}$: a neutron-diffraction and molecular-dynamics study, Phys. Rev. B 43 (1991) 1194–1197.
[43] C. Sonneville, A. Mermet, B. Champagnon, C. Martinet, J. Margueritat, D. de Ligny, T. Deschamps, F. Balima, Progressive transformations of silica glass upon densification, J. Chem. Phys. 137 (2012) 124505.
[44] M. Guerette, M.R. Ackerson, J. Thomas, F. Yuan, E. Bruce Watson, D. Walker, L. Huang, Structure and properties of silica glass densified in cold compression and hot compression, Sci. Rep. 5 (2015) 15343.
[45] A. Makishima, J.D. Mackenzie, Calculation of bulk modulus, shear modulus and Poisson's ratio of glass, J. Non-Cryst. Solids 17 (1975) 147–157.
[46] T. Rouxel, Elastic properties and short-to medium-range order in glasses, J. Am. Ceram. Soc. 90 (2007) 3019–3039.
[47] T. Rouxel, H. Ji, J.P. Guin, F. Augereau, B. Rufflé, Indentation deformation mechanism in glass: densification versus shear flow, J. Appl. Phys. 107 (2010) 94903.
[48] T. Deschamps, J. Margueritat, C. Martinet, A. Mermet, B. Champagnon, Elastic moduli of permanently densified silica glasses, Sci. Rep. 4 (2014) 7193.
[49] M.N. Svenson, M. Guerette, L. Huang, N. Lönnroth, J.C. Mauro, S.J. Rzoska, M. Bockowski, M.M. Smedskjaer, Universal behavior of changes in elastic moduli of hot compressed oxide glasses, Chem. Phys. Lett. 651 (2016) 88–91.
[50] K. Hirao, M. Yoshimoto, N. Soga, K. Tanaka, Densification of magnesium and calcium metaphosphate glasses, J. Non-Cryst. Solids 130 (1991) 78–84.
[51] K. Hirao, Z. Zhang, H. Morita, N. Soga, Effect of densification treatment on the mechanical properties of borate glasses, J. Soc. Mater. Sci., Jpn. 40 (1991) 400–404.
[52] S. Striepe, M.M. Smedskjaer, J. Deubener, U. Bauer, H. Behrens, M. Potuzak, R.E. Youngman, J.C. Mauro, Y. Yue, Elastic and micromechanical properties of isostatically compressed soda–lime–borate glasses, J. Non-Cryst. Solids 364 (2013) 44–52.
[53] A. Makishima, J.D. Mackenzie, Direct calculation of Young's moidulus of glass, J. Non-Cryst. Solids 12 (1973) 35–45.
[54] R.D. Shannon, Revised effective ionic radii and systematic studies of interatomic distances in halides and chalcogenides, Acta Crystallogr. A 32 (1976) 751–767.
[55] S. Inaba, S. Fujino, K. Morinaga, Young's modulus and compositional parameters of oxide glasses, J. Am. Ceram. Soc. 82 (1999) 3501–3507.
[56] C. Lin, L. Liu, Composition dependence of elasticity in aluminosilicate glasses, Phys. Chem. Miner. 33 (2006) 332–346.
[57] A.K. Swarnakar, A. Stamboulis, D. Holland, O. Van der Biest, T. Rouxel, Improved prediction of Young's modulus of fluorine-containing glasses using MAS-NMR structural data, J. Am. Ceram. Soc. 96 (2013) 1271–1277.
[58] R. Limbach, B.P. Rodrigues, D. Möncke, L. Wondraczek, Elasticity, deformation and fracture of mixed fluoride–phosphate glasses, J. Non-Cryst. Solids 430 (2015) 99–107.
[59] A. Pönitzsch, M. Nofz, L. Wondraczek, J. Deubener, Bulk elastic properties, hardness and fatigue of calcium aluminosilicate glasses in the intermediate-silica range, J. Non-Cryst. Solids 434 (2016) 1–12.
[60] R. Limbach, S. Karlsson, G. Scannell, R. Mathew, M. Edén, L. Wondraczek, The effect of TiO_2 on the structure of Na_2O-CaO-SiO_2 glasses and its implications for thermal and mechanical properties, J. Non-Cryst. Solids 471 (2017) 6–18.
[61] F. Yuan, L. Huang, Brittle to ductile transition in densified silica glass, Sci. Rep. 4 (2014) 5035.
[62] K.W. Peter, Densification and flow phenomena of glass in indentation experiments, J. Non-Cryst. Solids 5 (1970) 103–115.
[63] V. Keryvin, L. Charleux, R. Hin, J.-P. Guin, J.-C. Sangleboeuf, Mechanical behaviour of fully densified silica glass under Vickers indentation, Acta Mater. 129 (2017) 492–499.
[64] S. Yoshida, J.C. Sangleboeuf, T. Rouxel, Indentation-induced densification of soda-lime silicate glass, Int. J. Mater. Res. 98 (2007) 360–364.
[65] P. Sellappan, T. Rouxel, F. Celarie, E. Becker, P. Houizot, R. Conradt, Composition dependence of indentation deformation and indentation cracking in glass, Acta Mater. 61 (2013) 5949–5965.
[66] A. Winterstein-Beckmann, D. Möncke, D. Palles, E.I. Kamitsos, L. Wondraczek, A Raman-spectroscopic study of indentation-induced structural changes in technical alkali-borosilicate glasses with varying silicate network connectivity, J. Non-Cryst. Solids 405 (2014) 196–206.
[67] K.G. Aakermann, K. Januchta, J.A.L. Pedersen, M.N. Svenson, S.J. Rzoska, M. Bockowski, J.C. Mauro, M. Guerette, L. Huang, M.M. Smedskjaer, Indentation deformation mechanism of isostatically compressed mixed alkali aluminosilicate glasses, J. Non-Cryst. Solids 426 (2015) 175–183.
[68] K. Januchta, R.E. Youngman, A. Goel, M. Bauchy, S.J. Rzoska, M. Bockowski, M.M. Smedskjaer, Structural origin of high crack resistance in sodium aluminoborate glasses, J. Non-Cryst. Solids 460 (2017) 54–65.
[69] T. Rouxel, J.C. Sanglebœuf, J. Guin, V. Keryvin, G. Soraru, Surface damage resistance of gel-derived oxycarbide glasses: hardness, toughness, and scratchability, J. Am. Ceram. Soc. 84 (2001) 2220–2224.
[70] T. Rouxel, N. Dély, J.C. Sangleboeuf, S. Dériano, M. LeFloch, B. Beuneu, S. Hampshire, Structure–property correlations in Y–Ca–Mg–Sialon glasses: physical and mechanical properties, J. Am. Ceram. Soc. 88 (2005) 889–896.
[71] K. Li, J.C.M. Li, Y. Shapiro, Scratch test of soda-lime glass, Acta Mater. 46 (1998) 5569–5578.
[72] Y. Kato, H. Yamazaki, S. Yoshida, J. Matsuoka, Effect of densification on crack initiation under Vickers indentation test, J. Non-Cryst. Solids 356 (2010) 1768–1773.
[73] S. Striepe, J. Deubener, M. Potuzak, M.M. Smedskjaer, A. Matthias, J. Non-Cryst. Solids 445 (2016) 34–39.
[74] T.K. Bechgaard, A. Goel, R.E. Youngman, J.C. Mauro, S.J. Rzoska, M. Bockowski, L.R. Jensen, M.M. Smedskjaer, Structure and mechanical properties of compressed sodium aluminosilicate glasses: role of non-bridging oxygens, J. Non-Cryst. Solids 441 (2016) 49–57.
[75] S. Kapoor, N. Lönnroth, R.E. Youngman, S.J. Rzoska, M. Bockowski, L.R. Jensen, M.M. Smedskjaer, Pressure-driven structural depolymerization of zinc phosphate glass, J. Non-Cryst. Solids 469 (2017) 31–38.
[76] M. Ciccotti, Stress-corrosion mechanisms in silicate glasses, J. Phys. D. Appl. Phys. 42 (2009) 214006.